Magnetic properties of DyB2C, HoB2C, and ErB2C

Magnetic properties of DyB_2C, HoB_2C, and ErB_2C

Ryuta Watanuki* and Kazuya Suzuki
Graduate School of Environment and Information Sciences, Yokohama National University, 79-7 Tokiwadai, Hodogaya-ku, Yokohama 240-8501, Japan

Joost van Duijn
Department of Physics and Astronomy, Johns Hopkins University, Baltimore, Maryland 21218, USA and ISIS Neutron Facility, Rutherford Appleton Laboratory, Chilton, Didcot, Oxon OX11 0QX, United Kingdom

J. Paul Attfield
Centre for Science at Extreme Conditions and Department of Chemistry, University of Edinburgh, Kings Buildings, West Mains Road, Edinburgh EH9 3JJ, United Kingdom

(Received 27 September 2003; published 27 February 2004)

Magnetic properties of layered borocarbides RB_2C (R=Dy, Ho, and Er) have been studied by the magnetization and specific heat measurements at 1.8–300 K under the field up to 5 T. ErB_2C has a basic two-sublattice antiferromagnetic order below T_N=16.3 K. HoB_2C and DyB_2C show the three-dimensional magnetic order below T_C=7.0 K and 8.5 K, respectively. However, they have still large magnetic fluctuations below T_C. The magnetic ordering temperatures of RB_2C (R=Dy, Ho, and Er) do not follow the de Gennes relation, where the ordering temperatures of HoB_2C and DyB_2C are suppressed. The suppressions of ordering temperature and the unconventional fluctuating ground states of HoB_2C and DyB_2C originate from the spin frustration effects. The instability of the unconventional magnetic phase associated with the frustration is significant in this series; the fluctuating ground state results from the complex spin–spin interactions or spin–quadrupole interactions.

DOI: 10.1103/PhysRevB.69.064433 PACS number(s): 75.30.−m, 75.40.Cx, 75.50.Cc

I. INTRODUCTION

Layered metal borocarbides are of interest due to their low temperature electronic and magnetic properties. In recent years, it was discovered that DyB_2C_2 and HoB_2C_2 have an antiferroquadrupolar ordering at T_Q=24.7 K (Refs. 1,2) and 5.0 K,[3] respectively.

YB_2C-type structure described below is found for R=Sc, Y and Tb–Lu.[4–6] The YB_2C-type structure consists of alternating layers of rare earth metals and covalently bonded boron–carbon (B–C) sheets as shown in Fig. 1. The metal sheets are made of fused squares and triangles. The arrangement of the rare earth ions in RB_2C is topologically equivalent to the Shastry-Sutherland lattice.[7] The B–C sheets are formed by fused four- and seven-membered rings. Metal cations are situated below and above the centers of the seven-membered B–C rings. It was originally reported that successive B–C layers were rotated by 90° giving a tetragonal $P4_2/mbc$ structure,[4–6] however, a recent powder x-ray diffraction study of HoB_2C (Ref. 8) and a powder neutron diffraction study of ErB_2C have shown the possibility of a different structure model, where the B–C layers are stacked directly above each other leading to a orthorhombic $Pbam$ structure. The geometry of this B–C network can be derived from the tetragonal rare earth tetraboride RB_4 arrangement. A boron network of RB_4 consists of fused four- and seven-membered rings in the (001) plane. By removing the two out-of-plane boron atoms at the apices of the B_6 octahedral cluster, i.e., those that convert B_4 squares into B_6 octahedra, we obtain a hypothetical RB_3 stratified-structure. Substitution of the carbon atoms for the two of four boron atoms in the four-membered rings then gives the two-dimensional B_2C network system.

Recently, the low temperature neutron powder diffraction of DyB_2C, HoB_2C, and ErB_2C was investigated.[9] ErB_2C has two-sublattice antiferromagnetic order below 16.3 K. DyB_2C and HoB_2C show an unusual scattering in low wave number (Q) region. In HoB_2C, three peaks appear in low-Q range

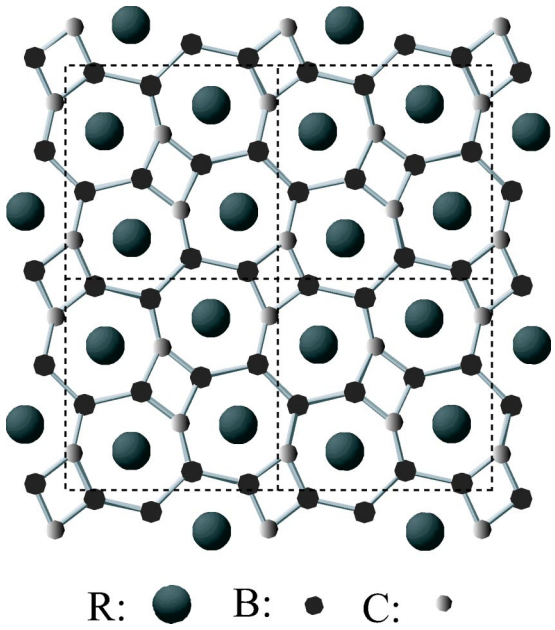

FIG. 1. Crystal structures of RB_2C (R=Dy, Ho, and Er) in a [001] projection.

between 8 and 16 K. Sharp peaks appear at 15.7 K and at 10.5 K, and a broad, asymmetric peak occur at 8 K. Those peaks are not typical spin wave or other magnetic superstructures, but can been explained by the formation of a Warren-type magnetic random layer (MRL) lattice. A conventional magnetic transition occurs at 7 K, although the unconventional correlations indicated by the low-Q peaks are maintained below this transition. The low temperature behavior of DyB_2C is very similar to that of HoB_2C. The origins of the unconventional properties are still unclear. Other physical properties of RB_2C have not been reported. In this paper, we report the magnetic behaviors of DyB_2C, HoB_2C, and ErB_2C studied by magnetization and specific heat measurements. The magnetic anisotropy of HoB_2C was examined using a single crystal.

II. EXPERIMENT

Polycrystalline samples of RB_2C (R=Dy, Ho, and Er) were prepared by an arc-melting method. Mixtures of powders of the starting materials, which were elemental rare earth metals (99.9% pure in powder), amorphous boron (99% pure, 1 micron powder size) and graphite (99% pure, 1–2 micron powder size), were compacted in stainless steel dies without the use of binders or lubricants. The 1 g pellets were arc-melted on a water-cooled copper hearth in an argon atmosphere. To obtain homogeneous samples, each melted button was turned over and remelted several times. The x-ray diffraction data were obtained on powdered samples with Cu-$K\alpha$ radiation, and confirm that the samples were single phase. A single crystal of HoB_2C was prepared by the Czochralski method in an argon atmosphere using a tetra-arc furnace.

The magnetizations of RB_2C were measured using a SQUID magnetometer (MPMS, Quantum Design Co.) in the temperature range of 1.8–300 K and under magnetic fields up to 5 T. The magnetic susceptibility measurements were performed after zero-field-cooled (ZFC) and after field-cooled (FC) conditions. For the single crystal of HoB_2C, the magnetization measurements, where the magnetic field H is applied parallel ($H \| c$) and perpendicular ($H \perp c$) to the c-axis, were carried out between 1.8 K and 300 K, and at several temperatures under magnetic fields up to 5 T. Specific heat measurements were carried out by a heat-relaxation method down to 1.9 K (using PPMS, Quantum Design Co.) and by a homemade light-irradiation AC method. The absolute value of the specific heat was obtained by the heat-relaxation method. The relative accuracy of the AC measurement is exceedingly high compared with that of the adiabatic or the heat-relaxation measurement, although the absolute value of specific heat cannot be estimated.

III. RESULTS AND DISCUSSION

A. ErB_2C

The temperature dependence of the magnetic susceptibility χ for a powder sample of ErB_2C measured in FC and ZFC conditions is shown in Fig. 2(a). The χ increases with decreasing temperature, and then passes through a peak at

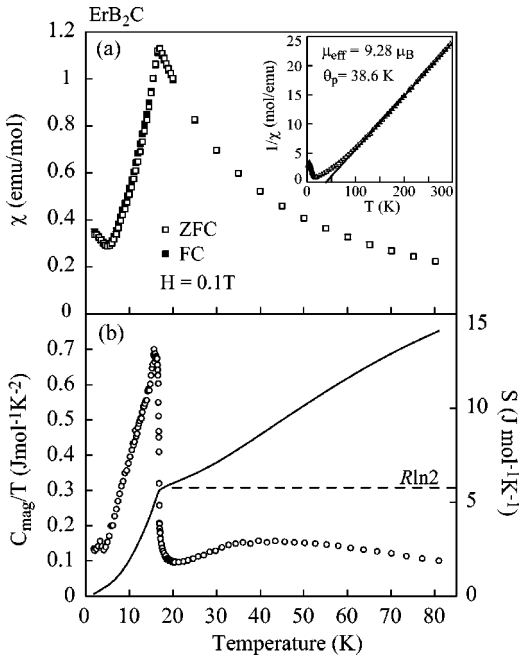

FIG. 2. (a) Magnetic susceptibility powder sample of ErB_2C. The inset shows the Curie–Weiss fit to the inverse susceptibility. (b) Magnetic specific heat divided by temperature C_{mag}/T (left axis) and corresponding entropy S (right axis) vs temperature for ErB_2C. The horizontal broken line indicates the value of entropy for the Kramers doublet.

16.7 K, and succeedingly it shows a minimum at 5.0 K. The peak of χ is attributed to the antiferromagnetic transition. The coincidence of the χ measured in FC and ZFC conditions suggests that no spontaneous magnetization appears in ErB_2C below T_N. This is consistent with the recent powder neutron diffraction study of ErB_2C, which found a collinear antiferromagnetic arrangement of the moments along the c axis.[9] However, the origin of the minimum of χ at 5.0 K is not clear.

The inverse molar susceptibility χ^{-1} [inset in Fig. 2(a)] shows Curie–Weiss behavior above 130 K. The effective paramagnetic moment (μ_{eff}) is estimated at 9.28 μ_B. Since this value is close to that expected for a free Er^{3+} ion value, 9.59 μ_B, the $4f$ electrons in ErB_2C are well localized. The Weiss temperature is θ_p=38.6 K. A nonlinear temperature dependence of χ^{-1} at low temperatures just above T_N may be due to crystal field effects.

The magnetization curves of the powder sample of ErB_2C (Fig. 3) were measured at 1.8 K, 5.0 K, 10.0 K, and 15.0 K under fields up to 5 T. The magnetization curve at 1.8 K shows a metamagnetic transition at the critical field of H_C =1.5 T. At higher temperatures, the transitions became smoother. The one-stepped field induced transition indicates that the ErB_2C has a basic two-sublattice antiferromagnetic structure, and a strong Ising-type anisotropy. The saturation magnetization of 7.4 μ_B/Er is less than a free Er^{3+} ion value gJ=9 μ_B/Er, where g is the Landé g factor and J is the total momentum of the f electron configuration.

The specific heat of the polycrystalline sample of ErB_2C shows a λ-like anomaly at T_N=16.3 K [Fig. 2(b)]. In addi-

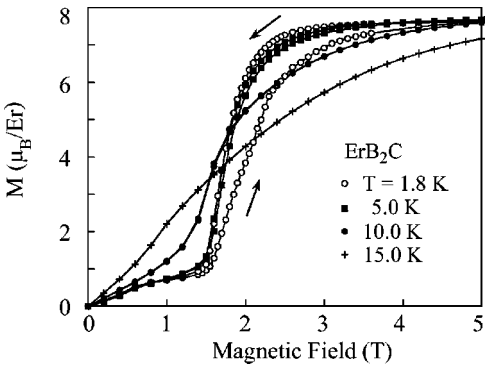

FIG. 3. Magnetization curves of the powder sample of ErB_2C at 1.8 K, 5.0 K, 10.0 K, and 15.0 K.

tion, a small anomaly in the specific heat data of ErB_2C is visible at 3.3 K, which corresponds to the minimum of the susceptibility. This may be due to a reorientation of the magnetic moment configuration. The temperature dependence of the magnetic specific heat divided by temperature C_{mag}/T measured by a heat-relaxation method is shown in Fig. 2(b). Subtracting the phonon component from the total specific heat, we obtain the temperature dependence of the magnetic specific heat. The phonon contribution was obtained from a measurement of the isostructural and nonmagnetic compound LuB_2C. We obtained the temperature dependence of the total entropy S by numerically integrating the data of C_{mag}/T vs T. Since our measurements are made above 1.9 K, only $\Delta S = S(T) - S(1.9\ \mathrm{K})$ can be obtained in this study. Therefore, we tentatively plot S putting $S(1.9\ \mathrm{K}) = 0$. The total entropy of approximately $R \ln 2$ is released around $T_N = 16.3$ K showing that Er here has a Kramers doublet ground state. The magnetic specific heat of ErB_2C shows a Schottky anomaly around 40 K, which is due to the crystalline electric field (CEF) splitting of the $J = 15/2$ multiplet of Er^{3+}.

B. HoB_2C

Figure 4(a) shows the magnetic susceptibility M/H for a single crystal of HoB_2C. The susceptibilities measured in the ZFC condition show a maximum at 7.0 K, while that in the FC condition shows weak increase below this temperature. The divergence of the FC and ZFC data may be ascribed to the appearance of weak spontaneous magnetization in HoB_2C. However, magnetization anomalies are not evident in the 8–16 K region, in which the unusual low-Q peaks are observed by the neutron diffraction.[9]

χ^{-1} of HoB_2C [Fig. 4(b)] follows the Curie–Weiss law above 40 K. The effective paramagnetic moments and the Weiss temperatures are estimated at $\mu_{\mathrm{eff}}^{\perp c} = 10.64\ \mu_B$ and $\theta_p^{\perp c} = -0.58$ K for $H \perp c$, and $\mu_{\mathrm{eff}}^{\parallel c} = 10.05\ \mu_B$ and $\theta_p^{\parallel c} = -4.75$ K for $H \parallel c$, respectively. The effective magnetic moment is close to the calculated value of 10.58 μ_B for a free Ho^{3+} ion. The negative values of θ_p indicate the existence of antiferromagnetic interactions. However, the small absolute values of θ_p, which are much less than the value of the magnetic ordering temperature, suggest the presence of competing interactions. The competition may originate from geometric spin frustration and may cause the unconventional properties observed in the neutron diffraction measurement of HoB_2C.[9]

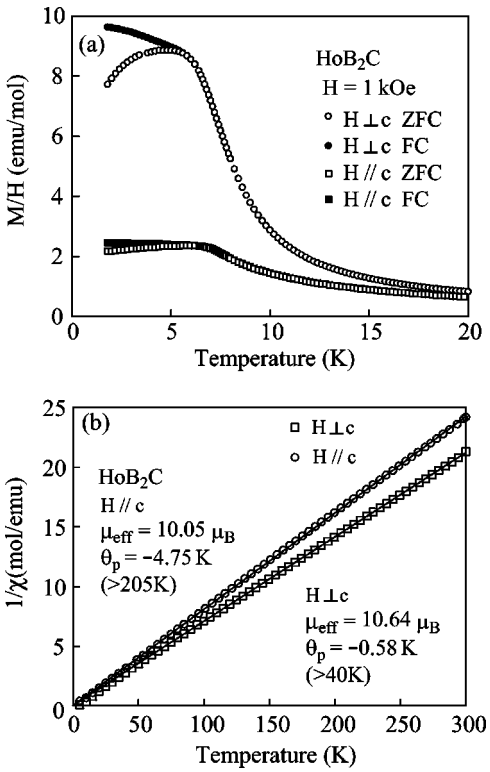

FIG. 4. (a) Magnetic susceptibility of HoB_2C. (b) Curie–Weiss fit to the inverse susceptibility.

Figure 5 shows the magnetization curves of the single crystal of HoB_2C at 1.8 K under a magnetic field up to 5 T, applied parallel and perpendicular to the c-axis. Below 1.5 T, the magnetization for $H \perp c$ was larger than the magnetization for $H \parallel c$. The anisotropic behaviors of the susceptibilities and the magnetization curves in the magnetic ordered phase indicate that the ordered magnetic moments favor to point within the (001) plane.

The spontaneous magnetization extrapolated to the zero field is estimated to be 4.7 μ_B/Ho for $H \parallel c$ and 4.4 μ_B/Ho for $H \perp c$. These values are less than half of the theoretical

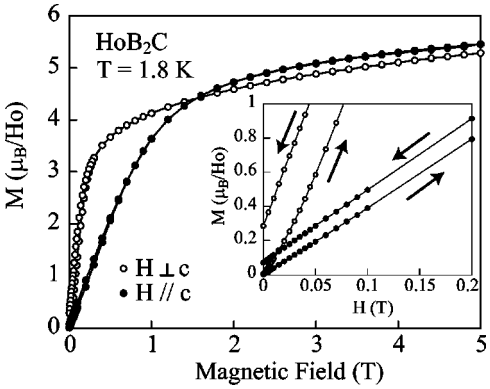

FIG. 5. Magnetization curve of HoB_2C. The inset shows an expanded view of the low field region.

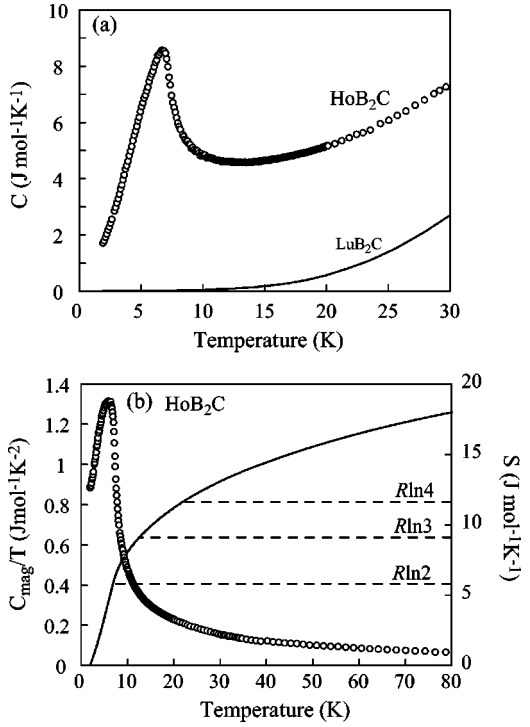

FIG. 6. (a) Specific heat of HoB_2C. The solid line represents the phonon and electron part determined from the specific heat of LuB_2C. (b) Magnetic specific heat divided by temperature C_{mag}/T (left axis) and corresponding entropy S (right axis) vs temperature for HoB_2C.

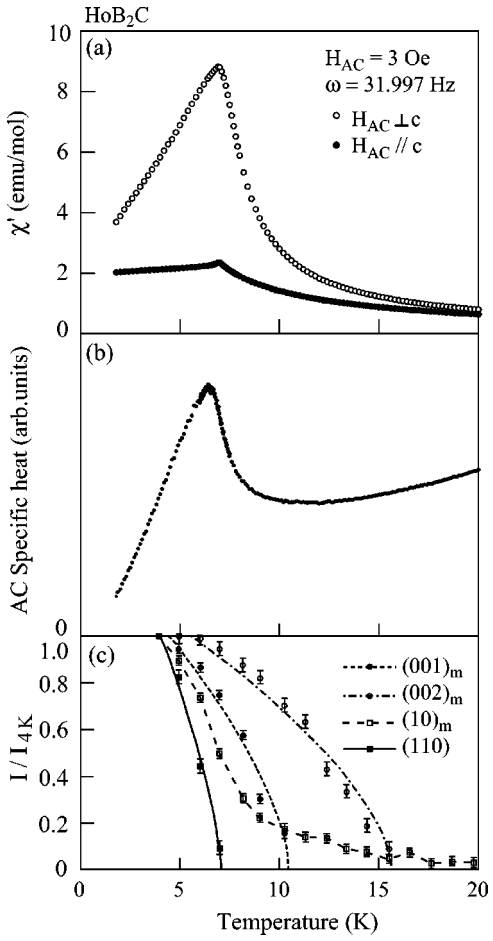

FIG. 7. (a) Real (filled symbols) part of AC susceptibility χ' for HoB_2C. H_{AC} is the amplitude of the driving field, ω is the driving frequency. (b) AC specific heat of HoB_2C. The AC-specific heat data in this figure are shown in an arbitrary scale. (c) Thermal evolution of the magnetic peak intensities (normalized to 4 K values) for HoB_2C (Ref. 9).

value of $gJ=10\ \mu_B$/Ho. The residual magnetizations for $H\perp c$ and $H\|c$ are 0.28 μ_B/Ho and 0.07 μ_B/Ho, respectively. The small values of the spontaneous magnetizations and the residual magnetizations suggest that HoB_2C is not an ordinary ferromagnet. The magnetic ordered state below 7.0 K is a canted antiferromagnetic one with a weak ferromagnetic component.

The specific heat of HoB_2C is shown in Fig. 6(a). A broad peak was observed at $T_C=7.0$ K, showing that HoB_2C has still large magnetic fluctuations in spite of the formation of three-dimensional magnetic order below T_C, since the shape of the peak is rather broader than a λ-type one usually observed in an ordinary magnet. This is consistent with the fact that the ordered magnetic moment in the conventional magnetic ordered phase is only 2.9 μ_B/Ho, which is about only a 29% of 10 μ_B/Ho is expected from $J=8$.[9] However, no anomalies in the specific heat or the susceptibilities were observed between 8 and 16 K. Moreover, the magnetic specific heat shows a tail in high temperature region, and the magnetic entropy is still released even far above $T_C=7.0$ K, as shown in Fig. 6(b).

In order to check for the existence of anomalies in the susceptibility and the specific heat between 8 and 16 K more precisely, AC measurements of the susceptibility and the specific heat was performed. Anomalies of the AC susceptibilities [Fig. 7(a)] and the AC specific heat [Fig. 7(b)] were not observed between 8 and 16 K by these measurements. The noncritical behavior of the specific heat between 8 and 16 K implies that the transition is not long-range order (LRO). In contrast, the temperature dependences of the integrated intensity of $(001)_m$ and $(002)_m$ neutron reflections [Fig. 7(c)] show the critical behavior between 8 and 16 K, respectively. Furthermore, the reflections widths of the $(001)_m$ and $(002)_m$ (the subscript m refers to the Warren-type MRL lattice) between 8 and 16 K indicate that the correlation length in the c direction is >1000 Å.[9] The result of the neutron diffraction study is contradictory to the result of the specific heat and the magnetization study. It is evident that the magnetic transition between 8 and 16 K are unconventional. Presumably, these transitions are invisible in the specific heat and the susceptibility since the entropy changes are small, and the anomalies may be broadened due to the nature of the MRL lattice.

C. DyB_2C

Figure 8 shows the magnetic susceptibility M/H for a powder sample of DyB_2C; these behaviors are similar to that of HoB_2C. The susceptibility measured in the ZFC condition

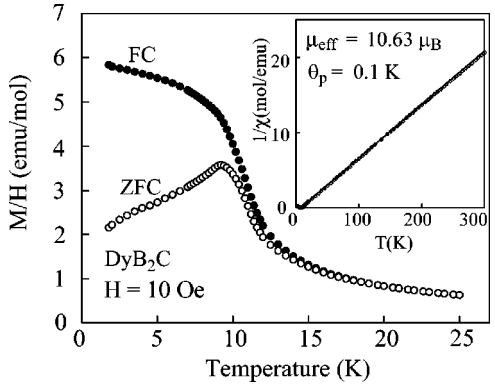

FIG. 8. Magnetic susceptibility of DyB_2C. The inset shows the Curie–Weiss fit to the inverse susceptibility.

shows a maximum at 9.2 K, while that in the FC condition shows weak increase below this temperature. It is possible that the divergence of the FC and ZFC data below 15 K illustrates the appearance of spontaneous magnetization of DyB_2C. However, no anomaly of the susceptibility around 22 K was observed.

H/M of DyB_2C (inset in Fig. 8) follows the Curie–Weiss law above 40 K, and the effective paramagnetic moment and Weiss temperature of DyB_2C are $\mu_{\text{eff}}=10.63\ \mu_B$ (which is identical to the value of a free Dy^{3+} ion) and $\theta_p=0.1$ K, respectively.

The magnetization curve of the powder sample of DyB_2C (Fig. 9) at 1.8 K under the field up to 5 T shows a ferromagnetic behavior. However, the spontaneous magnetization of 5.1 μ_B/Dy is only half of the theoretical value of $gJ=10\ \mu_B$/Dy. It seems likely that at least one more metamagnetic transition is occurs in high field regions above 5 T. The small values of the spontaneous magnetizations and the residual magnetizations suggest that DyB_2C is not an ordinary ferromagnet.

The specific heat of DyB_2C is shown in Fig. 10(a). A broad peak was observed at $T_C=8.5$ K and a very small hump around 20.5 K. The broad peak corresponds to the magnetic transition. DyB_2C has still large magnetic fluctuations in spite of the formation of three-dimensional magnetic order below $T_C=8.5$ K. This is consistent with the ordered magnetic moment being only 3.3 μ_B/Dy, whereas

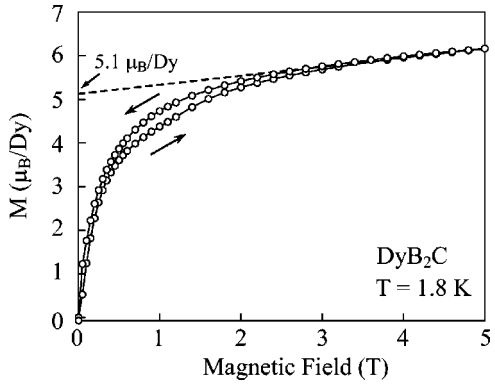

FIG. 9. Magnetization curve of DyB_2C.

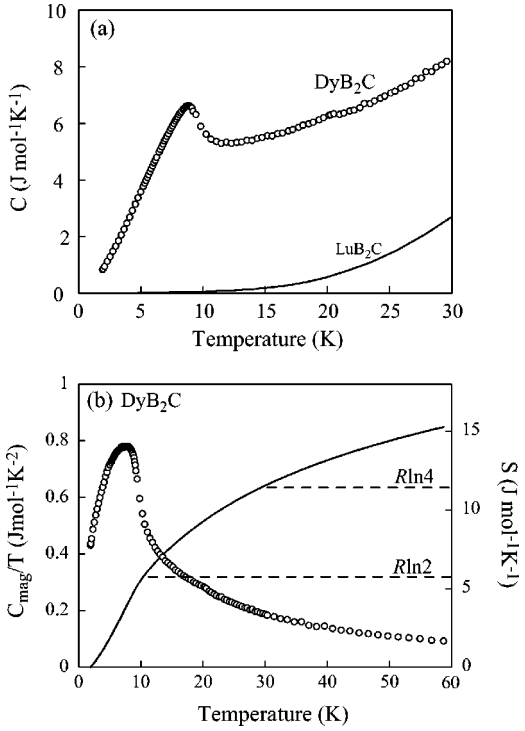

FIG. 10. (a) Specific heat of DyB_2C. The solid line represents the phonon and electron part determined from the specific heat of LuB_2C. (b) Magnetic specific heat divided by temperature C_{mag}/T (left axis) and corresponding entropy S (right axis) vs temperature for DyB_2C.

10 μ_B/Dy is expected from $J=15/2$.[9] Moreover, the magnetic specific heat shows a tail in high temperature region, and the magnetic entropy is still released even far above $T_C=8.5$ K, as shown in Fig. 10(b). The very small anomaly at 20.5 K coincides with the appearance of the sharp Warren $(002)_m$ peak observed by neutron diffraction measurements for DyB_2C.[9]

D. Magnetic ordering temperature

The magnetic properties of RB_2C ($R=$Dy, Ho, and Er) are summarized in Table I. The effective paramagnetic moments are close to those expected for a free R^{3+} ion values. These results indicate that the $4f$ electrons in the rare earth ions are well localized and the $4f$ levels locate far below the Fermi level (E_F). Hence, the influence of the $4f$-band hybridization with the conduction band at E_F is most likely very small. We believe that the density of states at E_F of RB_2C ($R=$Dy, Ho, and Er) does not so much change with rare earth element. Moreover, the neutron diffraction study of RB_2C ($R=$Dy, Ho, and Er) shows that the lattice constants and the interatomic distances between the rare earth ions change only 2% or less with the rare earth element.[9] Therefore, it is reasonable to assume that the magnetic coupling between the localized $4f$ moments in RB_2C is the Ruderman-Kittel-Kasuya-Yosida (RKKY) type one via conduction electron polarization, and the RKKY exchange coefficient remain unchanged for all rare earth elements in this series. In the RKKY model, magnetic transition temperatures

TABLE I. Magnetic properties of RB_2C (R=Dy, Ho, and Er). The magnetic transition temperatures T_C are determined by the temperature at the maximum of the specific heat. The Weiss temperature θ_p and the effective paramagnetic moment μ_{eff} are estimated from the Curie–Weiss fitting. $g\{[J(J+1)]^{1/2}$ is the effective paramagnetic moment of the free trivalent rare earth ion, where g is the Landé g factor and J is the total momentum of the f electron configuration. G is the de Gennes factor $G=(g-1)^2J(J+1)$.

Compound	T_C (K)	θ_p (K)	μ_{eff} (μ_B)	$g[J(J+1)]^{1/2}$ (μ_B)	G
DyB_2C	8.5	0.1	10.63	10.63	7.08
HoB_2C ($\perp c$)	7.0	−0.58	10.64	10.58	4.5
($\parallel c$)		−4.75	10.05		
ErB_2C	16.3 [a]	38.6	9.28	9.59	2.55

[a]Néel temperature T_N.

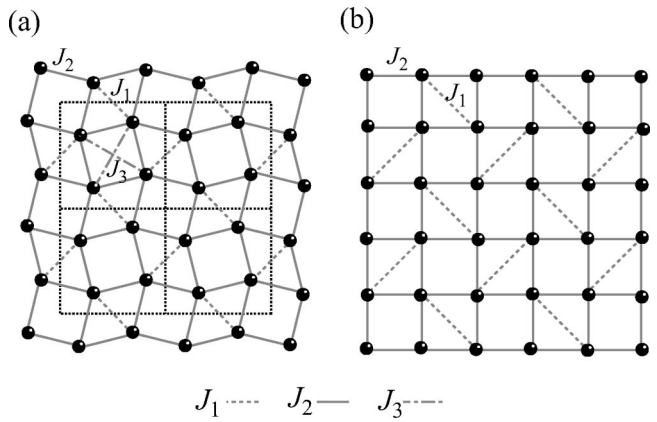

FIG. 11. (a) Lattice structure of the R^{3+} of RB_2C. Dotted line represents the unit cell. (b) The Shastry-Sutherland lattice.

are approximately proportional to the de Gennes factor $G=(g-1)^2J(J+1)$.[10] In RB_2C (R=Dy, Ho, and Er), however, the magnetic ordering temperatures do not follow the de Gennes relation. The disagree with the de Gennes scaling suggest that not only the RKKY interaction but also various mechanisms have to be considered when describing the magnetic coupling in RB_2C (R=Dy, Ho, and Er).

The magnetic susceptibilities and magnetization curves of HoB_2C suggest that the magnetic system of HoB_2C is anisotropic-Heisenberg-type. The magnetic system of DyB_2C is probably the same as that of HoB_2C. This is in a contrast to the Ising-type behavior in ErB_2C, where the magnetic moment lies parallel to the c-axis.[9] The magnetic anisotropies in RB_2C are due to CEF effects. It is natural that the increased degrees of freedom in the Heisenberg system lower the ordering temperature, because fluctuations are usually enhanced when the order parameter has continuous degrees of freedom. Therefore, the ordering temperatures of HoB_2C and DyB_2C are lower than those estimated from the de Gennes factor on the basis of ErB_2C.

The CEF has also considerable influence on the magnetic ordering temperature. Taking the CEF term added to the exchange Hamiltonian into account, the discrepancies between observed ordering temperatures and those predicted by the de Gennes relation was discussed.[11] The results of the inverse susceptibilities and the magnetic specific heat measurements of RB_2C (R=Dy, Ho, and Er) indicate that the CEF splitting of the low-lying levels of ErB_2C are larger than those of HoB_2C and DyB_2C. Thus, the magnetic ordering temperature of ErB_2C may be affected by CEF more strongly than those of HoB_2C and DyB_2C.

Magnetic ordering temperatures of the RB_2C_2 analogs also do not follow the de Gennes relation. The magnetic ordering temperatures T_N or T_C of TbB_2C_2, DyB_2C_2, HoB_2C_2, and ErB_2C_2 are 21.7 K, 15.3 K, 5.8 K, and 15.9 K, respectively.[1–3,12,13] The magnetic ordering temperatures of R=Tb, Dy, and Ho are suppressed by the competition between the quadrupole interaction and the magnetic interaction. It seems likely that the suppression of the ordering temperatures of HoB_2C and DyB_2C is also related to the quadrupole or/and higher multipole interaction of the $4f$ electrons.

E. Spin frustration in the Shastry-Sutherland lattice

In this section, we discuss the magnetic order in view of the geometric arrangement of the rare earth metals. The 2D-layer of the rare earth metals in RB_2C [Fig. 11(a)] is topologically equivalent to the Shastry-Sutherland model (SSM) [Fig. 11(b)], which is a 2D-model.[7] For the diagonal interaction J_1 and the square lattice interaction J_2, the Hamiltonian is written as

$$\mathcal{H}=J_1\sum_{\text{diagonals}}\boldsymbol{S}_i\cdot\boldsymbol{S}_j+J_2\sum_{\text{square}}\boldsymbol{S}_i\cdot\boldsymbol{S}_j. \tag{1}$$

This becomes a magnetically frustrated system if J_1 and J_2 are antiferromagnetic. In the Ising limit of SSM, the ground state for $J_1/J_2<2$ is the Néel LRO state ($(+-+-)$ structure) which is known to be the ground state of $\mathcal{H}$ for $J_1=0$, and that for $J_1/J_2>2$ is the "paramagnetic" dimer state, in which spins at the ends of a dimer bond must be antiparallel.

In the classical Heisenberg system of SSM, the phase diagram was exactly determined for Eq. (1) as a function of J_1/J_2. The phase diagram of the Heisenberg system of SSM differs greatly from that of the Ising system. For $J_1/J_2<1$, the Néel LRO state ($(+-+-)$ structure) is the ground state, whereas for $J_1/J_2>1$, the ground state is the helical LRO state with the incommensurate wave vector (π,q) or (q,π). With decreasing the spin S, the system falls into a quantum spin liquid state, where the dimer forms a spin singlet in the case of $J_1/J_2<0.7$ for $S=1/2$.[14]

1. *ErB_2C: Ising-type system*

The magnetic susceptibilities and magnetization curves of ErB_2C suggest that the magnetic system of ErB_2C is an Ising-type one. The neutron diffraction studies show that the magnetic structure of ErB_2C is a collinear $(+-+-)$ antiferromagnet as shown in Fig. 12, where the magnetic mo-

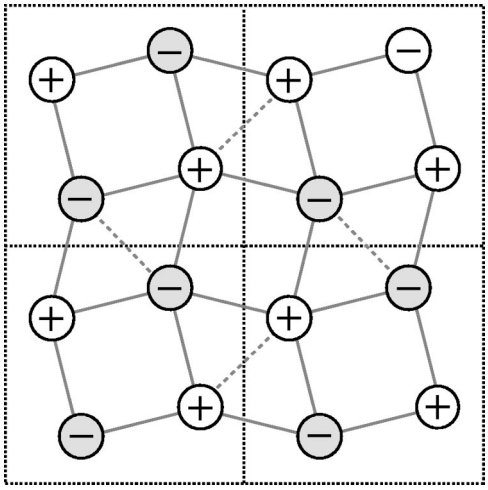

FIG. 12. Magnetic structure of the *c*-axis component for RB_2C (R=Dy, Ho, and Er).

ments lie parallel to the *c*-axis.[9] It is expected that the value of J_1 is close to that of J_2, since the triangular lattice of the rare earth metal of RB_2C is an almost equilateral triangle. This fact is consistent with the ground state of the Ising model for $J_1/J_2<2$ being the $(+-+-)$ LRO state. It is considered that the magnetic ordered state of ErB_2C corresponds to the Néel state for the Ising system of SSM.

2. *HoB_2C* and *DyB_2C*: Anisotropic Heisenberg-type systems

The magnetic properties of HoB_2C and DyB_2C are anisotropic-Heisenberg-type. The *c*-axis components of the small ordered magnetic moments below T_C adopt the collinear antiferromagnetic $(+-+-)$ structure.[9] As mentioned in the Secs. III B and III C, however, HoB_2C and DyB_2C have still large magnetic fluctuations in spite of the formation of the three-dimensional magnetic order below T_C. Moreover, the broad and asymmetric $(10)_m$ peak and the sharp $(001)_m$ and $(002)_m$ peaks in the low-Q region, which originate from a formation of the MRL lattice, are observed even below T_C by the neutron diffraction measurements of HoB_2C and DyB_2C. These facts imply that the basic Néel LRO state and the MRL state coexist below T_C. Because HoB_2C and DyB_2C belong to the anisotropic Heisenberg system, the phase boundary between the Néel state and the helical state may exist in the region $1<J_1/J_2<2$. Coexistence of the two magnetic states in HoB_2C and DyB_2C may be a critical phenomenon near the phase boundary for $1<J_1/J_2<2$ in the anisotropic Heisenberg system of SSM.

The Shastry-Sutherland theory does not include the magnetic fluctuations that appear in HoB_2C and DyB_2C. In the present case, additional interactions competing with J_1 and J_2 are necessary to explain the instability of the magnetic phase. The possible candidate is the diagonal coupling of the square lattices [J_3 in Fig. 11(a)]. For $J_2>0$ and $J_3>0$, the Shastry-Sutherland lattice is expected to be further frustrated. Thus the long-distance interaction J_3 seem to play an important role in the spin frustration, because the magnetic coupling between the localized $4f$ moments in the RB_2C is RKKY type. Furthermore, a quadrupole or/and higher multipole interaction of the $4f$ electrons competing with the magnetic interactions may be also related to the frustration of the magnetic fluctuations. A possible origin of the formation of the MRL lattice, which is characterized by the short in-plane magnetic correlation, is due to the formation of helical domains of SSM.

IV. CONCLUSION

We have studied the magnetic properties of RB_2C (R=Dy, Ho, and Er) by the magnetization and specific heat measurements. ErB_2C has a basic two-sublattice antiferromagnetic structure, and a strong Ising-type magnetic anisotropy. HoB_2C and DyB_2C show large magnetic fluctuations below T_C as well as the three-dimensional magnetic order. In RB_2C (R=Dy, Ho, and Er) both θ_p and the magnetic ordering temperatures do not follow the de Gennes relation, as HoB_2C and DyB_2C show a suppression of ordering temperature. The instability of the unconventional magnetic phase associated with the frustration is significant in this series; the fluctuating ground state results from the complex spin–spin interactions or spin–quadrupole interactions. For HoB_2C, no anomalies of the magnetizations and the specific heat are observed in the temperature region, in which the unusual low-Q peaks are observed by the neutron diffraction measurements. For DyB_2C, the magnetization anomalies are not evident, but the specific heat shows an anomaly in that region. The noncritical behavior of the specific heat in the temperature region implies the transitions are not LRO. The interesting magnetic properties of HoB_2C and DyB_2C may originate from the frustrated nature of the magnetic lattice containing triangular interactions between rare earth atoms. The specific ratio of the J_1, J_2, and J_3 interaction gives rise to complicate magnetic structures, one of which may bring about the formation of the MRL lattice. At present, however, we have insufficient information about the order parameter in these temperature regions. NMR and inelastic neutron scattering measurements will be performed to determined the spin dynamics of those unconventional materials.

*Email address: d01tb007@ynu.ac.jp

[1] H. Yamauchi, H. Onodera, K. Ohoyama, T. Onimaru, M. Kosaka, M. Ohasi, and Y. Yamaguchi, J. Phys. Soc. Jpn. **68**, 2057 (1999).
[2] K. Hirota, N. Oumi, T. Matsumura, H. Nakao, Y. Wakabayashi, Y. Murakami, and Y. Endoh, Phys. Rev. Lett. **84**, 2706 (2000).
[3] H. Onodera, H. Yamauchi, and Y. Yamaguchi, J. Phys. Soc. Jpn. **68**, 2526 (1999).
[4] J. Bauer and H. Nowotny, Monatsch. Chem. **102**, 1129 (1971).
[5] J. Bauer and J. Debuigne, J. Inorg. Nucl. Chem. **37**, 2473 (1975).
[6] J. Bauer, J. Less-Common Met. **87**, 45 (1982).
[7] B.S. Shastry and B. Sutherland, Physica B **108**, 1069 (1981).
[8] J. van Duijn, J.P. Attfield, R. Watanuki, and K. Suzuki, J. Phys. Chem. Solids **62**, 1423 (2001).
[9] J. van Duijn, J.P. Attfield, R. Watanuki, K. Suzuki, and R.K.

Heenan, Phys. Rev. Lett. **90**, 087201 (2003).
[10] P.G. de Gennes, J. Phys. Radium **23**, 510 (1962).
[11] D.R. Noakes and G. K. Shenoy, Phys. Lett. **91A**, 35 (1982).
[12] K. Kaneko, H. Onodera, H. Yamauchi, K. Ohoyama, A. Tobo, and Y. Yamaguchi, J. Phys. Soc. Jpn. **70**, 3112 (2001).
[13] K. Ohoyama, K. Indoh, A. Tobo, H. Onodera, and Y. Yamaguchi, J. Phys. Soc. Jpn. **71**, 1746 (2002).
[14] S. Miyahara and K. Ueda, Phys. Rev. Lett. **82**, 3701 (1999).